General Disclaimer

One or more of the Following Statements may affect this Document

- This document has been reproduced from the best copy furnished by the organizational source. It is being released in the interest of making available as much information as possible.

- This document may contain data, which exceeds the sheet parameters. It was furnished in this condition by the organizational source and is the best copy available.

- This document may contain tone-on-tone or color graphs, charts and/or pictures, which have been reproduced in black and white.

- This document is paginated as submitted by the original source.

- Portions of this document are not fully legible due to the historical nature of some of the material. However, it is the best reproduction available from the original submission.

NASA Technical Memorandum 79055

AERODYNAMIC PERFORMANCE
OF SCARF INLETS

John M. Abbott
Lewis Research Center
Cleveland, Ohio

AERODYNAMIC PERFORMANCE OF SCARF INLETS

by John M. Abbott

ABSTRACT

A scarf inlet is characterized by having a longer lower lip than upper lip leading to both aerodynamic and acoustic advantages. Aerodynamically, a scarf inlet has higher angle of attack capability and is less likely to ingest foreign objects while the aircraft is on the ground. Acoustically, a scarf inlet provides for reduced inlet radiated noise levels below the engine as a result of upward reflection and refraction of inlet radiated noise. Results of a wind tunnel test program are presented which illustrate the aerodynamic performance of two different scarf inlet designs. Based on these results, scarf inlet performance is summarized in a way to illustrate the advantages and limitations of a scarf inlet compared to an axisymmetric inlet.

INTRODUCTION

A scarf inlet is characterized by having a longer lower lip than upper lip. The motivation for designing an inlet in such a manner is to draw more airflow into the inlet from above than below, shifting the capture streamtube upward. This leads to several aerodynamic advantages as shown in figure 1. First, as indicated in figure 1(a), this orientation of the capture streamtube tends to unload the inlet lower lip (higher static pressure) and increase the loading on the upper lip (lower static pressure). Hence, as the inlet angle of attack is increased, and the lip loading shifts from the upper lip to the lower lip, the scarf inlet is able to attain a higher angle of attack (compared to an axisymmetric inlet wiyh the same lip shape) before the lower lip gets too highly loaded and the flow separates. Hence, higher inlet flow separation bounds are attainable with a scarf inlet.

Secondly, the orientation of the scarf inlet capture streamtube leads to a vertical velocity gradient within the inlet flow duct, that is, higher velocities in the upper portion of the duct and lower velocities in the lower portion. This velocity gradient serves to refract upward any forward propagating noise from the engine leading to reduced noise levels below the inlet toward the ground as indicated in figure 1(b). In addition, the physical presence of the

extended lower lip of the inlet acts as a noise barrier serving to reflect upward noise that would normally propagate downward. Hence, a scarf inlet is an effective noise redirecting inlet.

The third advantage offered by a scarf inlet is that the upward oriented capture streamtube tends to reduce the amount of foreign matter that is ingested into the engine. The inlet brings in a comparatively small percentage of its airflow in from below the engine where debris may be present on the runway (fig. 1(c)). Hence, the scarf inlet may lead to significant reductions in foreign object ingestion, a corresponding reduction in fan and compressor blade wear and an eventual reduction in the degradation in engine fuel economy associated with blade wear.

Because of the attractive advantages of a scarf inlet, a test program was undertaken to assess the low speed aerodynamic and acoustic performance of a scarf inlet. These tests were conducted in the Lewis Research Center's 9×15 Foot Low Speed Wind Tunnel with earlier results reported in references 1 and 2. These tests demonstrated the effectiveness of the scarf inlet in terms of both improved angle of attack capability and noise reduction below the inlet. However, these tests also revealed an undesirable characteristic of the inlet. The inlet was contoured such that the transition from the long lower lip to short upper lip resulted in a "corner" in the side profile. Because of the shape of the side profile of that inlet, it was referred to as a scoop inlet. The rapid change in inlet length in the region of this "corner" affected the aerodynamic performance of the scoop inlet by producing two vortices, one on each side of the inlet near the corners, which led to a performance penalty.

In order to eliminate this problem, a second scarf inlet was designed which had a straight side profile. That is, the transition from upper lip to lower lip was formed by a plane (see fig. 1). This eliminated the corners in the side profile and it was anticipated that this would lead to improved performance due to elimination of the vortices. The length of the lower and upper lips of the inlet was unchanged.

The aerodynamic performance of this straight scarf inlet (referred to subsequently as simply the scarf inlet) is the new material presented in this paper. Its performance is compared to that of the scoop inlet and a baseline axisymmetric inlet. All three inlets have the same lip shape and diffuser contour.

SYMBOLS

a	ellipse semi-major axis of internal lip
b	ellipse semi-minor axis of internal lip
D	diameter
DMAX	inlet total pressure distortion parameter (maximum total pressure − minimum total pressure)/(average total pressure)
L	length
M_t	one-dimensional throat Mach number
P	total pressure
p	static pressure
V	velocity
α	angle of attack
λ_{max}	maximum diffuser wall angle, deg
ψ	inlet circumferential position, deg

Subscripts:

c	centerbody
d	diffuser
e	diffuser exit
hℓ	highlight
max	maximum
ℓ	local
s	surface
sep	flow separation
t	throat
0	free-stream conditions
1	diffuser exit conditions

APPARATUS

Installation

The tests were conducted in the Lewis 9×15 Foot Low Speed Wind Tunnel (ref. 3). The test installation is shown in figure 2. A vacuum system was used in place of a fan or compressor to induce inlet flow. Inlet angle of attack was remotely varied by a turntable on which the test apparatus was mounted.

Inlet Design

The major variables defining the geometry of the baseline (axisymmetric) inlet, the scoop inlet and the scarf inlet are shown in figure 3. Each of the inlets has a diffuser-exit-diameter D_e of 30.48 centimeters with a one-dimensional design throat Mach number of 0.63. The main difference between the three inlets, of course, is that the inlet length L is dependent on circumferential location ψ for the scoop and scarf inlets and constant for the baseline inlet. Note that from circumferential angles of 113.6° to 246.4°, the scoop inlet length is constant and equal to that of the baseline inlet ($L/D_e = 0.716$). As the lower lip of the scoop is approached the length grows, through a lengthening of the inlet throat section, to a maximum value of $L/D_e = 1.295$. The scarf inlet length grows continuously from a value of $L/D_e = 0.716$ on the upper lip ($\psi = 180°$) to $L/D_e = 1.295$ on the lower lip.

For each of the three inlets the internal lip design is a 2-to-1 illipse with a relatively high area contraction ratio $(D_{h\ell}/D_t)^2$ of 1.44 to prevent internal flow separation at the relatively high angles of attack encountered in a STOL (short takeoff and landing) aircraft application. The external forebody design was selected for a cruise Mach number of 0.76 using design charts for symmetric inlets. This design would be expected to work quite well at cruise with the symmetric baseline inlet. However, the scoop and scarf inlets, with their asymmetric spillage properties at cruise, may require a different external forebody design.

INSTRUMENTATION AND DATA REDUCTION

Inlet aerodynamic performance was evaluated through use of static pressure taps on the inlet surfaces and total pressure rakes located at the inlet diffuser exit. Diffuser exit total pressure measurements were made using both

hub and tip boundary layer rakes as well as rakes spanning the entire annulus. Eight full-span total pressure rakes (equally spaced circumferentially) were used with six equal-area-weighted tubes per rake. The 16 boundary layer rakes (eight at the hub and eight at the tip) each contained five total pressure tubes.

Inlet total pressure recovery $P_{1,av}/P_0$ was computed using all measured total pressures, including boundary layer rakes, with the appropriate area weighting terms. However, in computing inlet total pressure distortion DMAX boundary layer measurements taken closer to the wall than the nearest tube on the six-element equal-area-weighted rakes were omitted. Inlet one-dimensional throat Mach number M_t was computed using the inlet weight flow measured by a venturi located downstream in the flow duct and the geometric throat area assuming uniform flow.

PROCEDURE

The test procedure consisted of setting free-stream velocity and inlet weight flow, and recording data at discrete angles of attack. Weight flow was then changed and data were taken again at the same discrete angles of attack. Finally, free-stream velocity was changed and the procedure was repeated over the weight flow and angle of attack range.

Data were also obtained on line to determine the angles of attack where inlet flow separation occurred. This was done by monitoring a lip surface static pressure and a diffuser exit total pressure, both on the windward side, as the angle of attack was steadily increased from 0°. This method has been used successfully in the past and is detailed in reference 4.

RESULTS AND DISCUSSION

Total Pressure Recovery and Distortion

The basic aerodynamic performance of the three inlets is compared in figure 4. The data are presented in a plot of inlet total pressure recovery against throat Mach number at static conditions (fig. 4(a)), and at a free-stream velocity of 41 meters per second with angles of attack of 0° (fig. 4(b)) and 50° (fig. 4(c)). In addition, at about the design throat Mach number of 0.63, values of total pressure distortion DMAX are shown in parentheses in each part of the figure.

At static conditions (fig. 4(a)) the total pressure recovery for each of the inlets is greater than 0.99 up to a throat Mach number of about 0.55. At throat Mach numbers above 0.55, however, the performance of the three inlets is considerably different. The baseline inlet recovery continues to drop at a steady rate with increasing throat Mach number as a result of increasing friction losses. At the maximum throat Mach number of 0.73, the recovery is 0.991.

The total pressure recovery for the scoop inlet, however, falls off at a faster rate as the throat Mach number is increased beyond 0.55. As explained in references 1 and 2, this lower level of recovery and higher distortion for the scoop inlet is a result of higher losses occurring over the upper portion of the inlet lip. The higher losses are due to the higher surface velocities over this portion of the lip resulting from the larger percentages of inlet airflow which is coming into the inlet from above (fig. 1). That is, the loading on the upper lip is considerably higher (the static pressures are lower) than that on the lower lip.

For the scarf inlet, the fall off in total pressure recovery at throat Mach numbers above 0.55 is even more pronounced. The reason for this fall off is the same as that given for the scoop inlet but because of the shape of the scarf side profile, the capture streamtube is shifted upward even further resulting in higher upper lip loading and an increase in losses over those encountered with the scoop inlet. In fact, at throat Mach numbers above 0.55, the upper lip becomes so highly loaded that the flow separates from the inlet upper lip leading to the low values of recovery and high value of distortion shown. Later discussions of the distribution of total pressure at the inlet diffuser exit plane and surface static pressure distributions for each of the three inlets will help to support these explanations.

With a free-stream velocity of 41 meters per second at an angle of attack of 0° (fig. 4(b)) the performance of both the scoop and the scarf inlets exhibits the same general trends as at static conditions, however, the fall off in recovery occurs at a throat Mach number of about 0.63. The reason for this improvement in performance for the scoop and scarf inlets with free-stream velocity is that the surface velocities (and hence losses) on the upper lip of the inlets are reduced as a result of a reduction in the percentage of inlet airflow that enters the inlet from above. That is, the free-stream velocity serves to distribute the lip loading more evenly between the top and bottom although it still remains biased toward the upper lip. The upper lip flow separation encountered at static conditions with the scarf inlet is no longer present.

An increase in angle of attack to 50° (fig. 4(c)) changes the picture considerably. The baseline inlet continues to perform well. The recovery for both the scoop and the scarf inlets now also remains high over the entire throat Mach number range. In addition, the scarf inlet has a higher recovery than the scoop inlet over the full range of throat Mach number.

The performance improvement for the scoop and scarf inlets at throat Mach numbers beyond 0.63 is a result of the shift in lip loading that occurs with increasing angle of attack. An increase in angle of attack serves to load the inlet lower lip and unload the upper lip. Hence, the high loading on the scoop and scarf inlet upper lip inherent at a 0° angle of attack, tends to be reduced as angle of attack is increased and the performance of the inlet improves accordingly.

The performance of the scarf inlet is now better than that of the scoop inlet because the straight side profile of the scarf does not lead to the formation of the two vortices formed in the "corners" of the scoop profile. This will become more evident in the following figures and discussion.

Total Pressure Distribution

Shown in figure 5 is the distribution of total pressure at the diffuser exit plane for the same three flow conditions; static (fig. 5(a)) and a free-stream velocity of 41 meters per second at angles of attack of 0° (fig. 5(b)) and 50° (fig. 5(c)). The distributions are shown at a throat Mach number of about 0.63.

At static conditions the distribution of total pressure for the scoop and the scarf inlet indicates the concentration of total pressure loss in the upper portion of the inlet duct due to the highly loaded upper lip. This is in contrast to the loss pattern of the baseline inlet which is concentrated in the outer wall boundary layer and axisymmetric.

The improvement in performance for the scoop and scarf inlets with a free-stream velocity of 41 meters per second and at a 0° angle of attack is evident in the total pressure distribution in figure 5(b). The scoop inlet total pressure distribution indicates that the losses are now smaller and are concentrated on the sides of the inlet duct at a circumferential position corresponding to the "corners" in the scoop side profile. As mentioned previously, these losses are believed to be a result of the formation of vortices in these "corners" which propagate back through the inlet. Note that for the scarf inlet these "corner" losses are not present and that the high loss region remains in the upper portion of the inlet duct, although the extent is reduced considerably.

Increasing angle of attack to 50° affects the distribution of total pressure as shown in figure 5(c). An increase in losses can be seen for the baseline inlet in the lower portion of the inlet duct as a result of the high lip loading (high surface velocities) on the lower lip at angle of attack. The losses associated with the two vortices in the scoop inlet are more evident now and have increased in magnitude. The losses for the scarf inlet are still located in the upper portion of the inlet duct but have decreased in magnitude over what they were at 0° angle of attack. Again, this is a result of the redistribution of inlet lip loading, that is, the effect of angle of attack is to make the asymmetric lip loading inherent in a scarf inlet at an angle of attack of 0° more symmetric.

Surface Static Pressure Distributions

The axial distribution of internal surface static pressure on the upper side of the inlets is shown in figure 6. The distributions are presented in a plot of the ratio of surface static to free-stream total pressure against axial distance downstream from the inlet highlight. Again, data are shown at static conditions (fig. 6(a)) and a free-stream velocity of 41 meters per second with angles of attack of 0° (fig. 6(b)) and 50° (fig. 6(c)). All data are shown at a throat Mach number of about 0.63 with one exception to be noted below.

At static conditions the high upper lip loading (low static pressure) is readily evident for the scoop and scarf inlets when compared to the baseline inlet. The pressure distribution for the baseline and scoop inlets is shown at a throat Mach number of 0.63. For the scarf inlet, the data is shown at a throat Mach number of 0.54 because, as previously mentioned, at higher throat Mach number the flow is separated from the upper lip.

At a free-stream velocity of 41 meters per second and 0° angle of attack (fig. 6(b)) the static pressure along the upper surface of each of the three inlets is equal to or greater than that at static conditions. This reduction in lip loading, and hence surface velocities, accounts for the improved performance of all three inlets noted in figure 4(b).

Increasing angle of attack to 50° (fig. 6(c)) has the effect of further increasing the static pressure on the upper lip of the three inlets and thereby improving the performance in this portion of the inlet duct. The lower surface of the inlet duct, for which no data are shown, is, of course, undergoing a decrease in static pressure (increase in loading) with increasing angle of attack thereby degrading the performance in the lower portion of the inlet

duct. The overall performance (total pressure recovery) of the entire inlet duct at a 50° angle of attack was illustrated in figure 4(c).

Figure 7 shows the circumferential distribution of surface static pressure at the highlight for the three inlets at the same flow conditions given in figures 4, 5, and 6. These distributions help to illustrate where the heavily loaded lip regions are located circumferentially and thereby where the critical flow regions are located.

At static conditions (fig. 7(a)) the distribution of static pressure around the highlight of the baseline inlet is constant as would be expected with an axisymmetric inlet. The distribution for the scoop inlet indicates the relatively high static pressure over the lower 60° of the inlet lip, corresponding to low lip loading, transitioning rather quickly to low static pressure (high loading) over the upper portion of the inlet lip (100° to 180°). The distribution for the scarf inlet indicates an almost steady decrease in static pressure (increase in loading) from lower to upper lip. As in figure 6, the data in figure 7(a) are for a throat Mach of 0.63 for the baseline and scoop inlets and 0.54 for the scarf inlet so that the comparison can be made with attached flow for each inlet. It is interesting to note that the lowest static pressure, corresponding to the most critical region for flow separation, occurs at the 96° position for the scoop inlet (corresponding to the location of the "corner" in the side profile) and at the 180° position for the scarf inlet.

At a free-stream velocity of 41 meters per second and angle of attack of 0° (fig. 7(b)) the increase in static pressure (decrease in loading) is clearly evident for all three inlets and this again is the reason for the improved performance with free-stream velocity first noted in figure 4. Note that the critical region (lowest static pressure) for the scoop inlet remains at the 96° position.

The effect of increasing angle of attack to 50° is shown in figure 7(c). The circumferential static pressure distribution for the baseline inlet has changed from being constant at 0° angle of attack to being lower at the 0° circumferential position and smoothly transitioning to higher at the 180° position. This is the expected effect of angle of attack on an axisymmetric inlet - higher loading on the lower lip and lower loading on the upper lip. The critical region for this inlet is, as expected, the inlet lower lip. Increasing the angle of attack to 50° with the scoop inlet leads to a shift in lip loading from the upper lip to the lower lip. But because the loading on the lower lip was relatively low at a 0° angle of attack, the lower lip loading at 50° angle of attack is not nearly as

great as that for the baseline inlet. Note that the critical region on the scoop continues to be at the 96° position and that it has become more critical (lower pressure) with this angle of attack increase.

In contrast, the circumferential pressure distribution for the scarf inlet has changed with increased angle of attack to the point where the lower lip of the scarf is now the critical position and the highest pressure (lowest loading) is on the upper lip. In fact the circumferential distribution is nearly flat at this position, similar to that for an axisymmetric inlet at 0° angle of attack.

Based on this discussion one may infer some expected results concerning the angle of attack where flow separation occurs for the three inlets and also the circumferential location of the separation. The inlet flow will become critical and separate when the lip static pressure drops to the point where the amount of diffusion becomes too large. For the baseline or any other axisymmetric inlet the critical region with increasing angle of attack is the lower lip as indicated in figure 7 (c). If the angle of attack were to be increased beyond 50°, the amount of diffusion would continue to increase and the flow would separate from the lower lip. With the scoop inlet one would expect that a higher angle of attack could be attained than with the baseline inlet, however, because of the critical region in the "corner" of the side profile the flow would separate in this region prior to attaining critical conditions on the lower lip. The scarf inlet, however, does not have the "corner" problem that the scoop does and instead the critical region is the lower lip. Since at any given angle of attack the flow conditions are less critical on the lower lip of the scarf inlet than on the lower lip of the axisymmetric baseline inlet or in the "corner" of the scoop inlet, it would be expected that the scarf inlet could attain a higher angle of attack before the lip flow separated. That is the subject of the next discussion.

Flow Separation Angle

At all flow conditions, the two flow separation indicators described in the PROCEDURE section indicated that the flow separation occurred on the inlet lower lip for each of the three inlets. (If it occurred in the inlet diffuser, which is possible, then it propagated immediately to the lip.) The separation data is shown in figure 8 where the angle of attack where lip flow separation occurs is plotted against inlet throat Mach number for each of the inlets. Data are shown at free-stream velocities of 41 meters per second (fig. 8(a)) and 61 meters per

second (fig. 8(b)). Below the data curves the flow is attached and above the flow is separated. At a free-stream velocity of 41 meters per second (fig. 8(a)), the inlets are ranked as expected from the previous discussion. At a given throat Mach number, as angle of attack is increased, the flow separates first on the baseline inlet. A higher angle of attack is attainable with the scoop inlet and even higher with the scarf inlet. In fact, at throat Mach numbers above 0.54, the flow remained attached up to an angle of attack of at least 140° which was the mechanical limit of the last rig. To reiterate the previous discussion, the scoop inlet is capable of higher angle of attack performance than the baseline inlet because of the inherently low loading on the lower lip at any given angle of attack. However, because of the "corner" in the side contour of the scoop inlet the flow condition becomes critical there first and flow separation occurs prior to the lower lip becoming critical. The scarf inlet has the highest angle of attack capability because it does not have the "corner" that the scoop does and the flow separates only when the lower lip becomes critical (which is at a much higher angle of attack than for the baseline inlet).

The same trends are observed at a free-stream velocity of 61 meters per second as shown in figure 8(b). The separation angles of attack for each of the three inlets are lower at this free-stream velocity because of the lower surface static pressures on the inlet lower lip (and hence, greater amount of diffusion) associated with turning the higher velocity free-stream flow into the inlet.

Summary and Suggested Improvements

The results presented in this paper indicate that with free-stream velocity, a scarf inlet can provide high angle of attack capability with high total pressure recovery and low distortion. At static conditions, however, this particular scarf inlet design encountered flow separation from the inlet upper lip.

From these results it can be inferred that for a symmetric inlet lip there is a trade between the length of the lower lip of the scarf, which serves to increase angle of attack capability, and the upper lip thickness or contraction ratio which is needed to provide good static performance for a given lower lip length. This trade is illustrated in figure 9 The figure is a plot of inlet lip contraction ratio $(D_{h\ell}/D_t)^2$ against length of the extension of the scarf lower lip in diffuser exit diameters L_{scarf}/D_e at a constant free-stream velocity and inlet throat Mach number. Shown in the figure are lines of constant angle of attack for lip flow separation α_{sep}. None of these variables are quantified in

the figure because with only one scarf inlet tested thus far, it is impossible to do so.

The figure indicates that at a given free-stream velocity and inlet throat Mach number, a required angle of attack for flow separation α_{sep} can be attained with lower inlet lip contraction ratios (and thereby thinner inlets), by increasing the length of the lower lip. This follows from the observation that extending the lower lip of the scarf shifts the capture streamtube upward and unloads the lower lip thereby reducing the lip thickness (contraction ratio) at which flow separation would occur for a given angle of attack. For a symmetric lip design this trade between increased lower lip extension and reduced contraction ratio for a given angle of attack capability cannot continue without limit, however, because at some point the inlet design will be such that upper lip flow separation will occur at static conditions. Hence, for a given amount of lower lip extension there is a minimum contraction ratio, dictated by the need for good static performance, as indicated by the crosshatched bound in the figure.

Note that the scarf inlet design which is discussed in this paper, is located to the right of this bound as a result of the upper lip flow separation encountered at static conditions. The figure suggests that in order to get satisfactory static performance for this inlet and maintain the same lower lip extension length, the lip contraction ratio must be increased. If the contraction ratio were to be increased around the entire circumference of the inlet, thereby keeping the lip symmetrical, the angle of attack capability would also improve as the figure indicates. It would, of course, only be necessary to increase the lip contraction ratio over some portion of the upper lip in order to attain satisfactory upper lip static performance. In this case the inlet lip would be asymmetric and the angle of attack capability of the inlet would not change since the lower lip contraction ratio was not changed.

Cruise Performance

At cruise conditions the spillage flow around the scarf inlet will be asymmetric. Because the lower lip is longer than the upper lip, the presence of upper lip is not sensed by the flow as soon as the lower lip at cruise conditions. Hence, less of the spillage airflow (that airflow which must pass around the inlet at cruise) is spilled over the lower lip than would normally spill for a symmetric inlet. This leaves more flow to be spilled over the upper lip. The inlet

external surfaces must be designed to account for this asymmetric spillage and avoid spillage flow separation or shock formation which would increase cruise drag.

An obvious way to design the inlet for this asymmetric spillage would be to vary the inlet external lip area circumferentially in order to provide more external surface for turning spillage flow on the top of the inlet than on the bottom as shown in figure 10(a). In this case, use may be made of external lip design charts developed for symmetric inlets, with some changes in interpretation.

Another method that might be used would be to contour the extended lower lip of the scarf inlet such that it followed the **shape of the bounding** streamline of the inlet capture streamtube (stagnation streamline) for a symmetric inlet at the same cruise condition as shown in figure 10(b). That is, instead of the lower lip extending straight forward, the lower lip would actually be curved upward thereby forcing flow to spill over the lower lip. Such a geometry would provide for a more equal circumferential distribution of spillage flow, however, its impact on overall inlet design and low speed aerodynamic and acoustic performance would need to be evaluated.

SUMMARY OF RESULTS

Wind tunnel tests were conducted to determine the aerodynamic performance of a scarf inlet. The results were compared to those from a baseline axisymmetric inlet and a scoop inlet. The results can be summarized as follows:

1. The straight side profile of the scarf inlet eliminated the aerodynamic performance penalties associated with the vortices created in the "corners" of the scoop inlet side profile.

2. At static conditions, flow separation occurred on the upper lip of the scarf inlet at throat Mach numbers above 0.55. A free-stream velocity of 41 meters per second improved upon the static performance of the scarf inlet and eliminated the upper lip flow separation.

3. At all values of free-stream velocity and inlet throat Mach number, the scarf inlet attained a higher angle of attack before lip separation than did the scoop or baseline inlets.

4. The contraction ratio on the upper lip of the scarf inlet reported on here was too small for the amount of lower lip extension leading to upper lip flow separation at static conditions. An increase in upper lip contraction ratio should eliminate this separation problem.

5. The flow spillage about a scarf inlet at cruise is asymmetric with more flow being spilled over the inlet upper lip than lower lip. The inlet external lip must be designed to account for this characteristic.

REFERENCES

1. Abbott, J. M., "Aeroacoustic Performance of a Scoop Inlet," AIAA Paper 77-1354, Oct. 1977.

2. Abbott, J. M., and Dietrich, D. A., "Aerodynamic and Directional Acoustic Performance of a Scoop Inlet," NASA TP-1028, 1977.

3. Yuska, J., Diedrich, J. H., and Clough, N., "Lewis 9- by 15-Foot V/STOL Wind Tunnel," NASA TM X-2305, 1971.

4. Luidens, R. W., and Abbott, J. M., "Incidence Angle Bounds for Lip Flow Separation of Three 13-97-Centimeter-Diameter Inlets," NASA TM X-3351, 1976.

E-9865

C-77-4497

Figure 2. - Test installation in 9- by 15-foot wind tunnel.

AXISYMMETRIC INLET

SCARF INLET

$\alpha = 0^0$

$\alpha = 50^0$

(a) HIGHER FLOW SEPARATION BOUNDS.

INCREASING SPL, dB
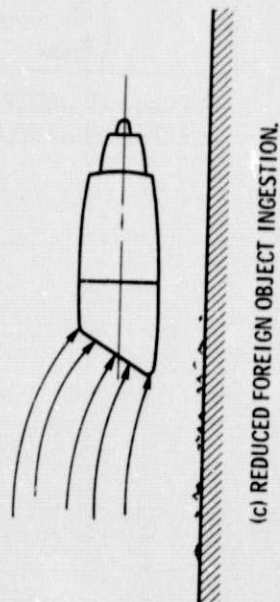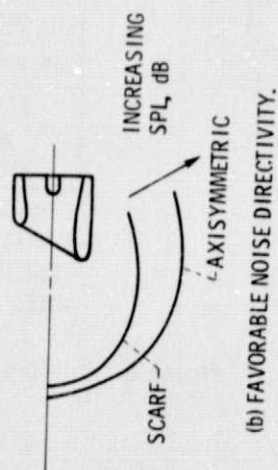
AXISYMMETRIC

SCARF

(b) FAVORABLE NOISE DIRECTIVITY.

(c) REDUCED FOREIGN OBJECT INGESTION.
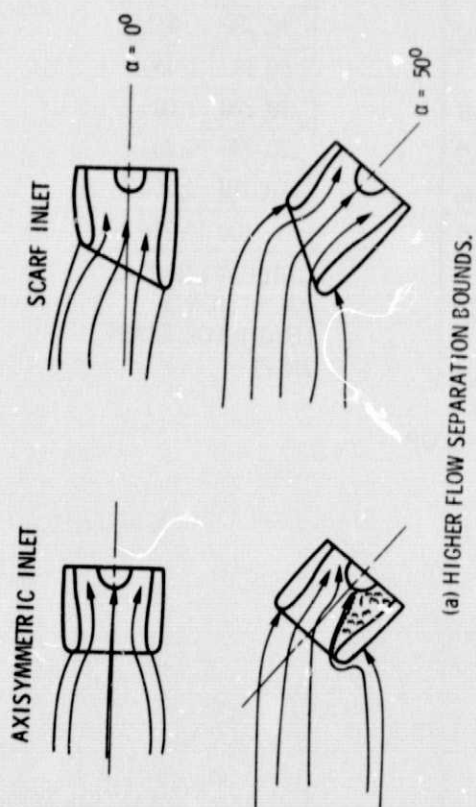
Figure 1. - Advantages of a scarf inlet.

DESIGN PARAMETERS; SCOOP, SCARF, AND BASELINE INLETS
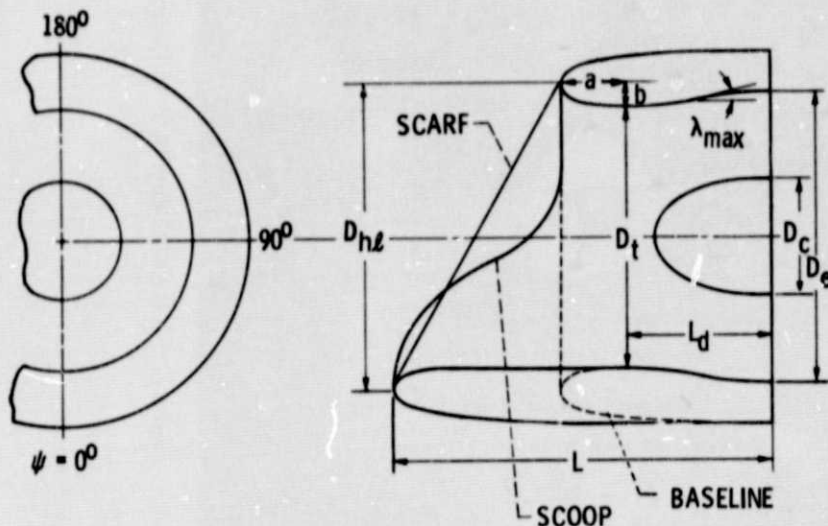
LIP	$(D_{h\ell}/D_t)^2$	1.44
	a/b	2.0
DIFFUSER	$(D_e - D_c)^2/D_t^2$	1.048
	L_d/D_e	0.538
	λ_{max}	8.37°

ψ, deg	L/D_e
0	1.295
30, 330	1.290
45, 315	1.266
60, 300	1.207
90, 270	0.823
100, 260	0.746
105, 255	0.727
113.6 ↓ 296.4	0.716

CIRCUMFERENTIAL VARIATION OF LENGTH FOR SCOOP INLET

ψ, deg	L/D_e
0	1.295
30, 330	1.256
60, 300	1.150
90, 270	1.005
120, 240	0.860
150, 210	0.754
180	0.716

CIRCUMFERENTIAL VARIATION OF LENGTH FOR SCARF INLET

Figure 3. - Inlet design.

SCARF

SCOOP

BASELINE

$P_{1,\ell}/P_0$ .99

.99

.82

.96

$\psi = 0^0$

(a) FREESTREAM VELOCITY, V_0 0.

.99

.96

.99

(b) FREESTREAM VELOCITY, V_0 41 METERS PER SECOND; ANGLE OF ATTACK, α, 0^0.

.96

.99

.99

.96

.99

.96

V_0

(c) FREESTREAM VELOCITY, V_0 41 METERS PER SECOND; ANGLE OF ATTACK, α, 50^0.

Figure 5. – Distribution of total pressure at diffuser exit plane. Inlet throat Mach number, M_t ~0.63.

TOTAL PRESSURE DISTORTION, DMAX

0.02   .15   .22

(a) FREESTREAM VELOCITY, V_0 0.

.05   .01   .14

(b) FREESTREAM VELOCITY, V_0 41 METERS PER SECOND; ANGLE OF ATTACK, α, 0^0.

.04   .03   .15

(c) FREESTREAM VELOCITY, V_0 41 METERS PER SECOND; ANGLE OF ATTACK, α, 50^0.

THROAT MACH NUMBER, M_t

.3   .4   .5   .6   .7   .8

1.00   .98   .96   .94

TOTAL PRESSURE RECOVERY, $P_{1,av}/P_0$

Figure 4. – Inlet aerodynamic performance.

○ BASELINE
□ SCOOP
△ SCARF

(a) FREESTREAM VELOCITY, V_0, 0.

(a) FREESTREAM VELOCITY, V_0, 41 METERS PER SECOND; ANGLE OF ATTACK, α, 0°.

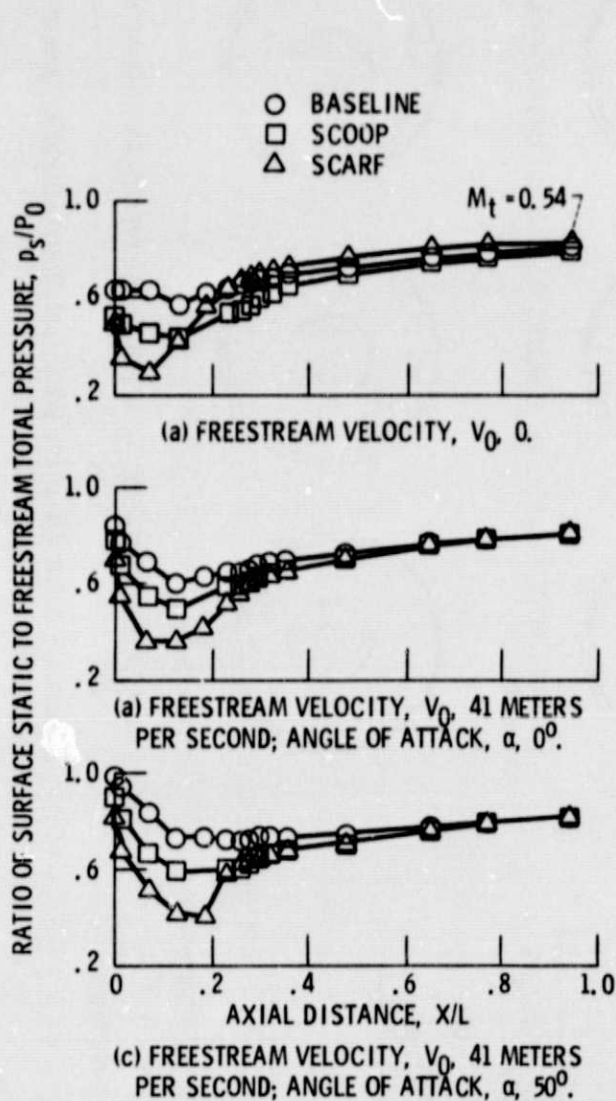(c) FREESTREAM VELOCITY, V_0, 41 METERS PER SECOND; ANGLE OF ATTACK, α, 50°.

Figure 6. - Axial distribution of surface static pressure on inlet leeward side (ψ = 180°). Inlet throat Mach number, M_t, 0.63 except as indicated.
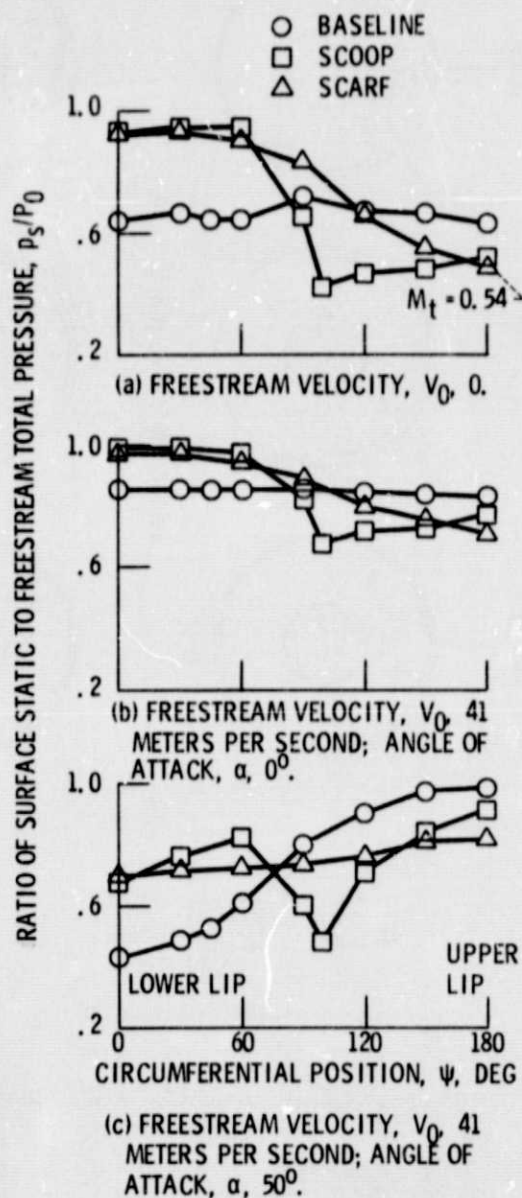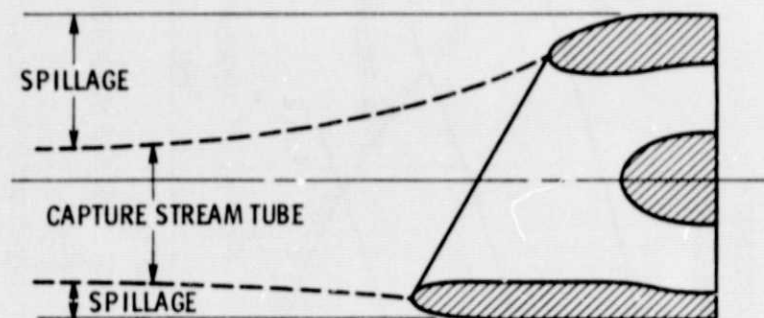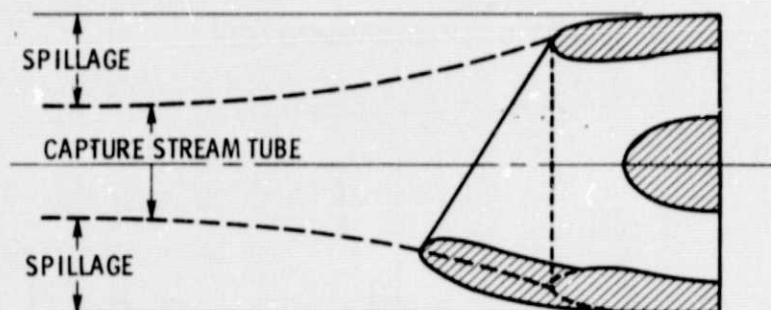
○ BASELINE
□ SCOOP
△ SCARF

(a) FREESTREAM VELOCITY, V_0, 0.

(b) FREESTREAM VELOCITY, V_0, 41 METERS PER SECOND; ANGLE OF ATTACK, α, 0°.

(c) FREESTREAM VELOCITY, V_0, 41 METERS PER SECOND; ANGLE OF ATTACK, α, 50°.

Figure 7. - Circumferential variation of surface static pressure at highlight. Inlet throat Mach number, M_t, 0.63 except as indicated.

Figure 9. - Summary of scarf inlet low speed performance.

(a) FREESTREAM VELOCITY, V_0, 41 METERS PER SECOND.

(b) FREESTREAM VELOCITY, V_0, 61 METERS PER SECOND.

Figure 8. - Inlet flow separation bounds.

(a) ASYMMETRIC EXTERNAL LIP.

(b) CONTOURED LOWER LIP.

Figure 10. - Cruise design.